Intensity of singular stress field (ISSF) variation as a function of the Young's modulus in single lap adhesive joints

doi: https://doi.org/10.1016/j.ijadhadh.2019.102418

Intensity of singular stress field (ISSF) variation as a function of the Young's modulus in single lap adhesive joints

Pedro Galvez[1,2], Nao-Aki Noda[1]*, Rei Takaki[1], Yoshikazu Sano[1], Tatsujiro Miyazaki[3], Juana Abenojar[2], Miguel Angel Martínez[2]

[1]Department of Mechanical Engineering, Kyushu Institute of Technology, 1-1 Sensui-cho Tobata-ku Kitakyushu-shi, Fukuoka 804-8550, Japan

[2]Materials Science and Engineering and Chemical Engineering Department, University Carlos III de Madrid, Avenida de la Universidad 30, 28911, Leganes, Spain

[3]Department of Mechanical Systems Engineering, University of the Ryukyus, 1 Senbaru, Nishihara-cho Nakagami-gun, Okinawa 903-0213, Japan

Abstract

The use of mixed adhesive joints has proven to be very useful. This type of joint allows improving the performance by increasing the strength and decreasing the stresses in critical areas of the joint. In the same way, the use of the Intensity of Singular Stress Field (ISSF) has demonstrated to be suitable for the calculation of adhesive joints, since the adhesive strength can be controlled by the ISSF at the interface end. Four finite element models have been created by combining two epoxy adhesives with different mechanical properties, and therefore with different Young's modulus. New mixed adhesive joints have been compared with respect to only-one adhesive joints in terms of ISSF. Results show a clear improvement with one of the

configurations of mixed adhesive joints. A significant decrease of 35.64% of the ISSF is obtained compared to the only-one adhesive configuration.

Keywords: Intensity of singular stress field; strength evaluation; fracture mechanics; finite element stress analysis

Nomenclature

Symbols

E	Young's Modulus
$K_{\sigma c}$	Critical ISSF
υ	Poisson's Ratio
σ_{ys}	Steel yield strength
σ_{fs}	Steel tensile strength
ε_{fs}	Steel elongation at break
σ_{fa}	Adhesive tensile strength
ε_{fa}	Adhesive elongation at break
G	Shear modulus
T_A	Adhesive thickness
L_0	Adhesive overlap

W_A	Single lap joint specimen width
T_S	Steel substrate thickness
L_S	Steel substrate length
L_T	Specimen length
L_{0A1}	Adhesive 1 overlap
L_{0A2}	Adhesive 2 overlap
K_σ, K_τ	ISSF
r	Radial distance away from the singular point
$f_{\theta\theta}(\theta, \lambda_k), f_{r\theta}(\theta, \lambda_k)$	Non-dimensional functions of angle θ and λ_k
α, β	Dundurs′ material parameters
θ	Angle from the interface corner
λ	Singular index
σ_y, τ_{xy}	Tension and shear stress component near the crack tip
σ_0	Tension at both ends of single lap joint
τ_{ave}	Average shear stress at fracture
$\sigma^*_{y0,FEM}, \tau^*_{xy0,FEM}$	FEM stresses at the interface corner of the reference problem
$\sigma_{y0,FEM}, \tau_{xy0,FEM}$	FEM stresses at the interface corner of the unknown problem

Abbreviations

FEM	Finite elements method
ISSF	Intensity of Singular Stress Field
RWCIM	Reciprocal work contour integral method

1. Introduction

The great development in the adhesives field during the last decades has allowed their use in very diverse industries such as automotive, aerospace, construction, electronics, packaging and sports [1]. Adhesives provide several advantages over other traditional mechanical joints, highlighting: lower density and costs, homogeneous distribution of loads and ability for corrosion protection among others. The increasingly widespread use of adhesives makes necessary the development and use of techniques capable of accurately assessing their behavior and ability. Finite element methods (FEM) have proved to be a very effective tool in the calculation of adhesive joints. Xará and Campilho [2] determine that extended Finite Element Method, using different initiation criteria, is a precise and proper tool for the strength prediction of single-L joints bonded with either brittle or ductile adhesives. Li et al. [3] and Noda et al. [4] say that the adhesive strength can be controlled by the intensity of the singular stress field (ISSF) at the interface end, and also the strength of the lap joint can be given as $K_{\sigma c} = const$. Mintzas and Nowell [5] say that the strength of the adhesive bond can be expressed as $H_{cr} = const$. Thus logical and efficient ISSF methods can be applied to evaluate the adhesive strength, since it is proven that the ISSF may control it. Wang and Rose [6] developed a novel

work in which compact solutions of the corner singularity at the adhesive/adherent interface in a bonded lap joint are shown. A numerical matched asymptotic expansion method is used to determine the stress intensity factors for the limiting case of rigid substrates. The suitability of the analytical solutions is proven since they are capable of bring good representations of the singular stress fields at the adhesive/substrate corners with respect to the results obtained by finite elements using a fine mesh near the corner points. Goglio and Rossetto [7] demonstrate the existence of a relationship between stress intensity factor and peak structural stresses in the adhesive at the overlap ends. They propose a procedure to estimate the stress intensity factor without the need for a detailed finite element analysis of the joints. The equations of the problem are solved by a valid numerical procedure. The suitability of the procedure is evaluated for single lap joints by combining different values of joint parameters, establishing the type of stress that should be considered to obtain the correct definition of the stress intensity factor.

UNE-EN 1465 and JIS K6850 are the Spanish and Japanese standards that detail how to calculate the adhesive strength in lap joints. Nevertheless the specimen configuration affects significantly to the lap joint strength, and therefore this strength cannot be expressed as $\tau_{ave} = const$, as it is indicated by Li et al. [3]. Ideal single lap joint tests are intended to be conducted under pure shear loading, but actually the existence of other loads is well known in the literature, causing the appearance of other efforts such as peeling [8]. Maximum peeling stress is located within the adhesive bond near the adhesive-adherent interface at the corner edge, as it is demonstrated by Martinez et al. [9]. Li et al. [10] say that ISSF at the interface corner is related with the peeling force, and in the same way peeling force directly depends of the adhesive stiffness and the adhesive thickness. The stiffness effect on the ISSF is discussed,

focusing on how to minimize the ISSF in single lap joint specimens by mean of the combination of one higher Young's modulus and one lower Young's modulus epoxy adhesives. Incorporate different adhesives (with different mechanical properties) to the bond line can improve the stress distribution and also can reduce these stresses. The literature shows other works with mixed adhesive joints such as the joints proposed in this work. Chiminelli et al. [11] say that by using the mixing adhesive approach to create new mixed adhesive joints, the ultimate load can be increased by 70% respect to the base adhesives assemblies. Breto et al. [12] have been studied the singularity impact by mean of two independent methodologies for selecting the intermediate material between adhesive bands in mixed adhesive joints. Fitton et al. [13] show the effect of variable modulus bondlines in single lap joints, concluding that this kind of joints are able to reduce stress concentration, increase the strength of the joint, reduce the experimental scatter and even change the mode of failure. da Silva et al. [14] compare mixed adhesive joints with joints only manufactured with a brittle adhesive, obtaining higher joint strength for mixed adhesive joints. The best adhesive joint combination in this work is composed by one ductile adhesive at the ends of the overlap, and one brittle adhesive in the central area. Carbas et al. [15] have been created an induction heating method to manufacture adhesively bonded functionally graded joints obtaining a performance improvement close to 70%.

Despite there are several related researches, as it has been seen previously, none of these works have studied the effect of Young's modulus in non-mixed and mixed adhesive joints in terms of the Intensity of Singular Stress Field (ISSF). Four single lap joint models are

developed in this work, combining two epoxy adhesives with different mechanical properties, studying the behaviour in terms of ISSF of each model.

2. Specimen design

2.1 Materials

In this work structural AISI 4140 alloy steel was selected for both substrates. The main mechanical properties of this steel are: Young´s modulus (E_s) of 210 GPa, yield strength (σ_{ys}) of 415 MPa, tensile strength (σ_{fs}) of 655 MPa, elongation at break (ε_{fs}) of 25.70% and Poisson´s ratio (υ_s) of 0.3. Two structural epoxy adhesives (SikaPower®-1511 and SikaPower®-1548) were considered. Table 1 shows the mechanical properties of the adhesives highlighting the difference in the values of the Young's modulus. Being a purely theoretical article, manufacturer mechanical properties of the AISI 4140 alloy steel and the adhesives were used to perform the simulation.

Table 1. Manufacturer mechanical properties of SikaPower®-1511 and SikaPower®-1548.

Property	SikaPower®-1511	SikaPower®-1548
Young´s modulus, E_a [GPa]	3.3	1.0
Poisson´s ratio, υ_a	0.367	0.396
Tensile strength, σ_{fa} [MPa]	45.0	30.0
Elongation at break, ε_{fa} [%]	3	9
Shear Modulus, G [GPa]	1.21	0.36

2.2 Specimen Geometry

Single lap joint configuration was selected to calculate ISSF. Two different configurations of single lap joint were used. First one with a completely homogeneous adhesive layer, using a

unique adhesive. Second one using two adhesives, one adhesive for the corners, and other adhesive for the central area. Representation and dimensions of both single lap joint configurations can be seen in Fig 1. The chosen dimension for the Single Lap Joint specimens were (in mm): adhesive thickness (T_A) = 0.2, adhesive overlap (L_0) = 25, adhesive and steel width (W_A) = 25, steel thickness (T_S) = 25, steel length (L_S) = 100, specimen length (L_T) = 175, adhesive 1 overlap (L_{0A1}) = 15, adhesive 2 overlap (L_{0A2}) = 5. Da Silva et al. [16] demonstrated that adhesive thickness of 0.2 mm is the most suitable value in terms of the lap shear strength of epoxy adhesives. In Ref [3], the effect of adherent steel thickness T_s on the ISSF was investigated under the same tensile load. Then, it was found that the ISSF decreases with increasing T_s and becomes constant when $T_s \geq 25$mm. This is because the bend deformation of the single lap joint becomes smallest under $T_s \geq 25$mm. For this reason, 25 mm of steel substrate thickness were chosen to carry out this work.

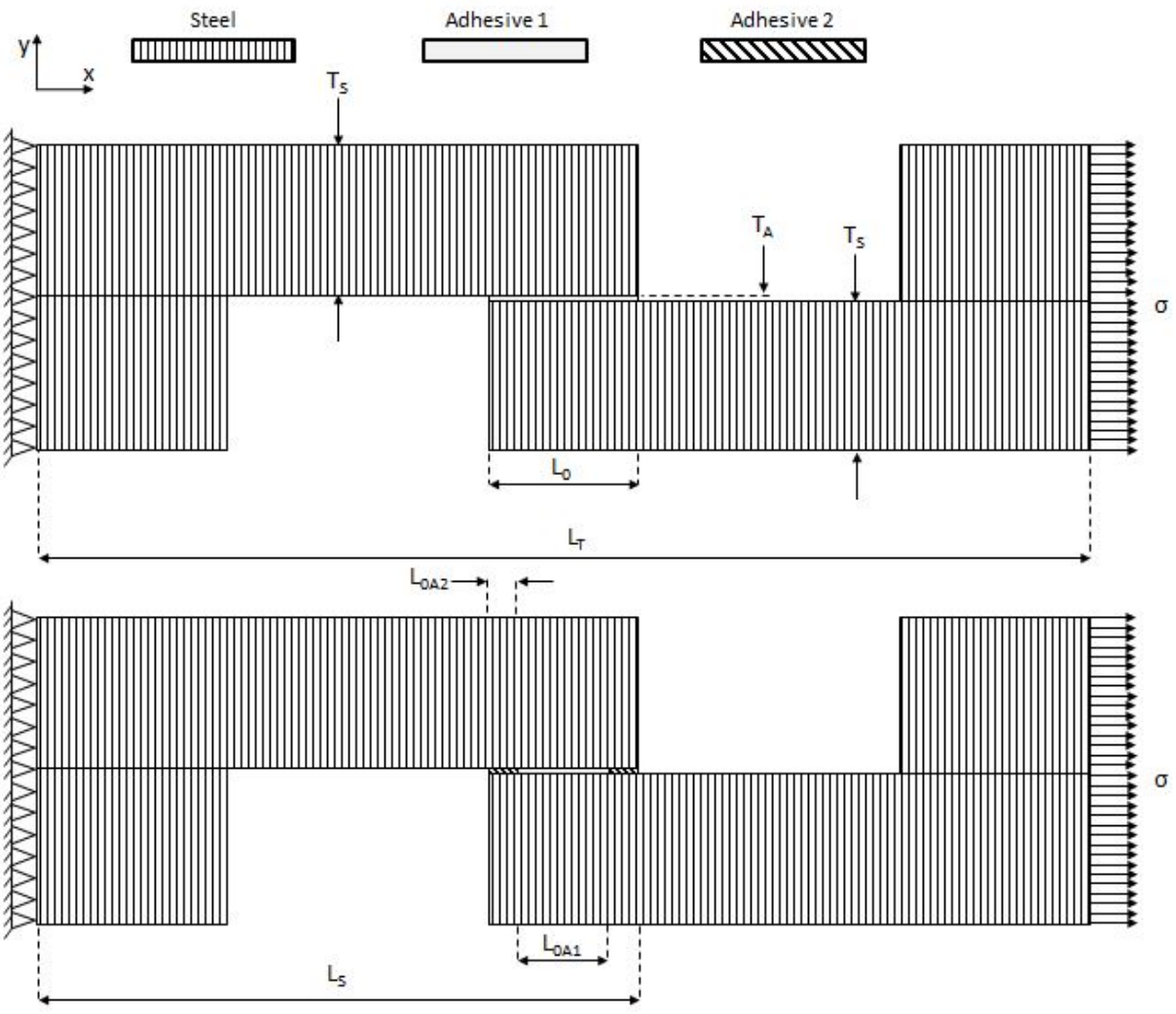

Figure 1. Representation of studied single lap joint configurations.

Four models were studied combining the properties of both SikaPower®-1511 and SikaPower®-1548 adhesives. In Model 1 and Model 2, homogeneous layers of the SikaPower®-1511 and SikaPower®-1548 were used respectively. In Model 3 and Model 4 both adhesives were combined. SikaPower®-1548 was used in the corners and SikaPower®-1511 in the center in Model 3, while in Model 4 the opposite was carried out. Adhesive configurations of the models are shown in Fig 2.

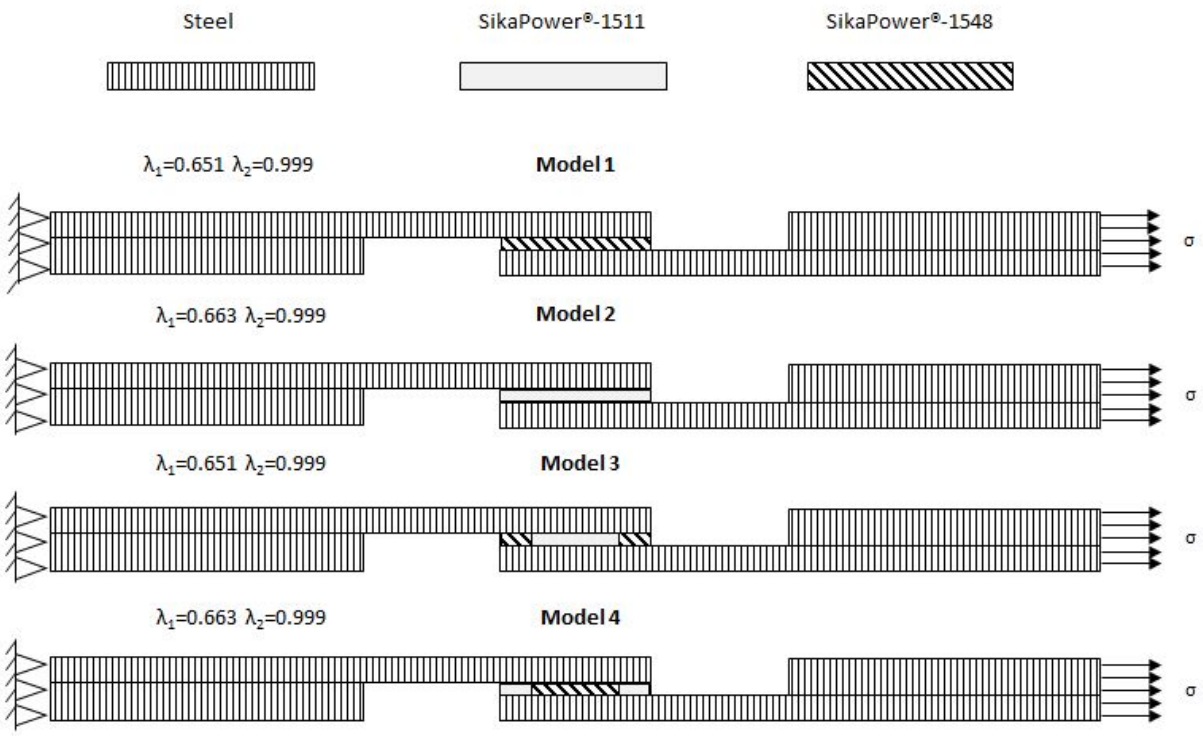

Figure 2. Adhesive configurations of the studied models.

3. Calculation of ISSF

Intensity of singular stress field (ISSF) was used to evaluate the effect of the Young's Modulus in single lap joints. ISSF method is described in this section. Zhang et al. [17, 18] showed the ability of mesh-independent techniques to calculate the ISSF. α and β are the parameters of Dundurs [19], which are defined by the shear modulus G_m and by the Poisson's ratio υ_m, being m = a for the adhesive and m = s for the substrate. α and β were calculated from Eq 1 and Eq 2:

$$\alpha = \frac{G_a(k_s + 1) - G_s(k_a + 1)}{G_a(k_s + 1) + G_s(k_a + 1)} \quad (1)$$

$$\beta = \frac{G_a(k_s - 1) - G_s(k_a - 1)}{G_a(k_s + 1) + G_s(k_a + 1)}$$

(2)

k_m was calculated from Eq 3:

$$k_m = \begin{cases} \dfrac{3 - \upsilon_m}{1 + \upsilon_m} \\ 3 - 4\upsilon_m \end{cases}$$

(3)

Where ${3 - \upsilon_m}/{1 + \upsilon_m}$ is relative to the plane stress and $3 - 4\upsilon_m$is relative to the plane strain. In this work, the effect of the Young's Modulus was discussed in terms of the ISSF. Noda et al. [20] say that this is possible since in 2D modelling, the adhesive strength can be expressed as a constant value of the ISSF. Singular index (λ) characterizes the singular stress field in lap joints, and it was calculated from eigenequation (Eq 4), which was derived by Bogy [21], and proves two real roots for majority of material combinations [3, 4]:

$$4sin^2(\pi\lambda)\left\{sin^2\left(\frac{\pi\lambda}{2}\right) - \lambda^2\right\}\beta^2 + 4\lambda^2 sin^2(\pi\lambda)\alpha\beta + \left\{sin^2\left(\frac{\pi\lambda}{2}\right) - \lambda^2\right\}\alpha^2 - 4\lambda^2 sin^2(\pi\lambda)\beta - 2\left\{\lambda^2 cos(2\pi\lambda) + sin^2\left(\frac{\pi\lambda}{2}\right)cos(\pi\lambda) + \frac{1}{2}sin^2(\pi\lambda)\right\}\alpha + sin^2\left(\frac{3\pi}{2}\lambda\right) - \lambda^2 = 0$$

(4)

Regarding the boundary conditions (Fig 3), fixed tensile stress $\sigma = 1\ MPa$ was selected. This tensile stress is corresponding to a load parameter (P/W) of 50.2 N/mm. The load parameter was calculated from Eq 5:

$$\frac{P}{W} = \sigma T$$

(5)

Where P is the load, W is the specimen width (25 mm), σ is the tensile stress (1 MPa) and T is the total thickness of the specimen (50.2 mm). Total thickness was calculated from $T = (2T_s) + T_A$, being T_S the substrate thickness and T_A the adhesive thickness. σ=1MPa was selected in all models to perform the simulation under the same conditions.

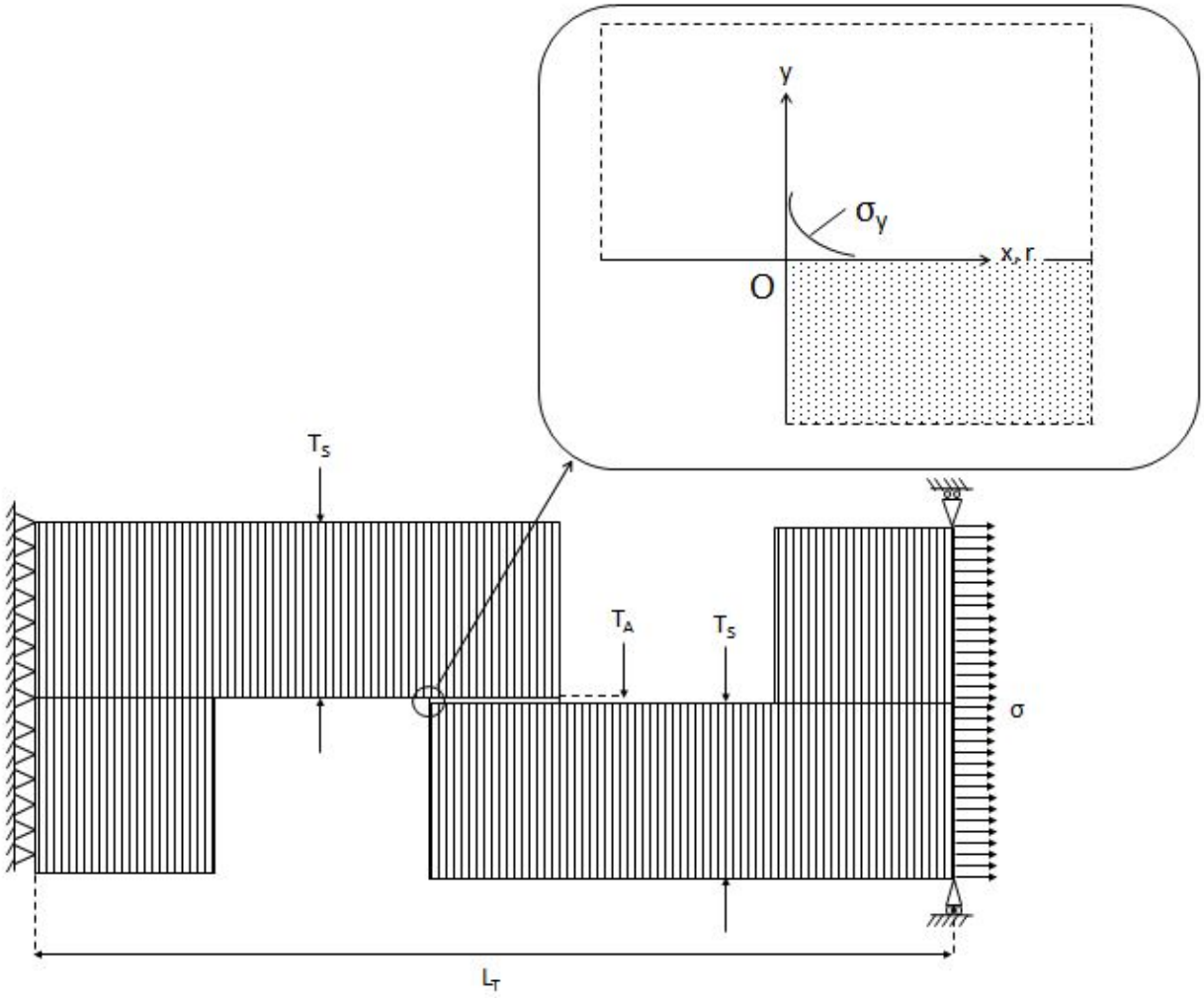

Figure 3. Boundary conditions: σ = 1 MPa, P/W = 50.2 N/mm, T_A = 0.2 mm, T_S = 25 mm, W = 25 mm, L_T = 175 mm.

By setting σ=1 MPa as boundary condition reliable qualitative analysis can be ensured. Analogous models (those with the same materials combination in the edge corner) can be correctly compared.

Continuing with the theoretical framework, the stresses σ_y and τ_{xy} that are located around the interface end can be expressed as follows:

$$\sigma_y = \frac{K_{\sigma,\lambda_1}}{r^{1-\lambda_1}} + \frac{K_{\sigma,\lambda_2}}{r^{1-\lambda_2}} \cong \frac{K_{\sigma,\lambda_1}}{r^{1-\lambda_1}}\left(1 + C_\sigma r^{\lambda_2-\lambda_1}\right)$$

$$\tau_{xy} = \frac{K_{\tau,\lambda_1}}{r^{1-\lambda_1}} + \frac{K_{\tau,\lambda_2}}{r^{1-\lambda_2}} \cong \frac{K_{\tau,\lambda_1}}{r^{1-\lambda_1}}\left(1 + C_\tau r^{\lambda_2-\lambda_1}\right) \quad (6)$$

Where r is the radial distance away from the corner singular point O. In previous studies [17, 18, 20, 22], the strength of butt joints was also expressed as a constant value independent of the adhesive thickness although the boundary is straight instead of notch shape. Therefore, in previous studies [3, 4], the term of ISSF (Intensity of Singular Stress Field) has been used instead of notch stress intensity factors defined for notches [23]. In Eq (6), $K_{\sigma,\lambda1}$ and $K_{\sigma,\lambda2}$ are the values of ISSF. C_σ and C_τ are two ratios which are almost constants except for extreme geometries of adhesive [20], and were calculated following Eq 7. In Ref [4], the adhesive strength of the single lap joints can be expressed as a constant value of ISSF except in the case of very short adhesive overlap length. If $\lambda_2 \approx 1$ the effect of $K_{\sigma,\lambda_2}/r^{1-\lambda_2}$ and $K_{\tau,\lambda_2}/r^{1-\lambda_2}$ becomes very small in Eq 6. Thus ISSFs are commanded only by $K_{\sigma,\lambda1}$ and $K_{\tau,\lambda1}$, being both values the expression of ISSF parameters, as was explained in previous works [4].

$$C_\sigma = \frac{K_{\sigma,\lambda_2}}{K_{\sigma,\lambda_1}}$$

$$C_\tau = \frac{K_{\tau,\lambda_2}}{K_{\tau,\lambda_1}}$$

(7)

In this work the value of ISSF had been calculated in four different models (Fig 2). Materials combination in the edge corner must be the same to be able to compare two models. Therefore, Model 1 could be compared with Model 3, and Model 2 could be compared with Model 4, since in both cases the combination of materials in the corner singular point was the same. Fig 4 shows material combination of Model 1 – Model 3 and Model 2 – Model 4 in the corner singular point O. In Ref [3, 4], the adhesive strength of lap joint is expressed as a constant value of the ISSF (K_σ) independent of the adhesive geometry. Therefore, the strength of Model 1 and Model 3 can be compared in terms of ISSF since they have the same singular stress field having the same singular index λ (λ1=0.651, λ2=0.999 as it is shown in Figure 2 and Table 2). In a similar way, the strength of Model 2 and Model 4 can be compared in terms of ISSF since they have the same singular stress field having the same singular index λ (λ1=0.663, λ2=0.999 as it is shown in Figure 2 and Table 3).

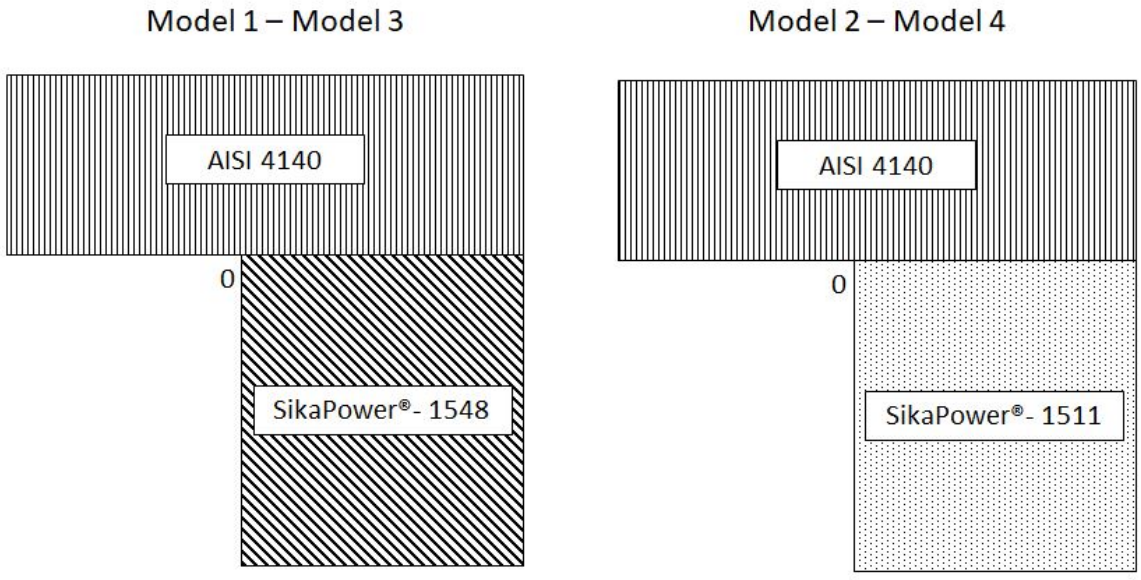

Figure 4. Material combination in Model 1 – Model 3 and Model 2 – Model 4.

$K^*_{\sigma,\lambda1}$ and $K^*_{\tau,\lambda1}$ are the reference solutions, while the unknown solutions had been designated as $K_{\sigma,\lambda1}$ and $K_{\tau,\lambda1}$. The stress distribution obtained by means of finite elements method (FEM) are designated as $\sigma^*_{y0,FEM}$ and $\tau^*_{y0,FEM}$ for the reference solutions and $\sigma_{y0,FEM}$ and $\tau_{y0,FEM}$ for the unknown solutions. Therefore, from Eq 6 the ratios $K_{\sigma,\lambda1}/K^*_{\sigma,\lambda1}$ and $\sigma_{y0,FEM}/\sigma^*_{y0,FEM}$ can be indicated as it is shown in Eq 8:

$$\frac{K_{\sigma,\lambda_1}}{K^*_{\sigma,\lambda_1}} = \frac{\sigma_{y0,FEM}}{\sigma^*_{y0,FEM}} \tag{8}$$

Eq 8 is valid if the reference value is known, and as long as the same mesh pattern had been applied in the FEM models in both reference and unknown solutions. Analogously, the same kind of equation can be used to calculate $K_{\tau,\lambda 1}$ (Eq 9):

$$\frac{K_{\tau,\lambda_1}}{K^*_{\tau,\lambda_1}} = \frac{\tau_{xy0,FEM}}{\tau^*_{xy0,FEM}} \tag{9}$$

In this work, ISSF values for Models 1 and 2 had been selected as reference values. Since there is no work in the bibliography with this combination of materials, specimen configuration and boundary conditions, both reference values were calculated by mean of the Reciprocal Work Contour Integral Method (RWCIM) [4, 24], which details are shown in Appendix A.

Stresses σ_θ and $\tau_{r\theta}$ in the r direction around interface corner O in Fig 3 can be expressed as:

$$\sigma_\theta = \frac{K_1}{r^{1-\lambda_1}} f_{\theta\theta}(\theta,\lambda_1) + \frac{K_2}{r^{1-\lambda_2}} f_{\theta\theta}(\theta,\lambda_2)$$

$$\tau_{r\theta} = \frac{K_1}{r^{1-\lambda_1}} f_{r\theta}(\theta,\lambda_1) + \frac{K_2}{r^{1-\lambda_2}} f_{r\theta}(\theta,\lambda_2) \tag{10}$$

Where r is the radial distance away from the corner singular point O. K_k (k=1,2) has real values; $f_{\theta\theta}(\theta,\lambda_k)$ and $f_{r\theta}(\theta,\lambda_k)$ are non-dimensional functions of angle θ and λ_k. There are three boundaries in a bi-material open wedge such as the one shown in Fig 3, two traction-free edges

(at angles θ=-π/2 and θ=π) and one in the interface (θ=0). If the focus is on the interface stress, four parameters control the intensity of singular stress fields (ISSFs):

$$K_1 f_{\theta\theta}(\theta,\lambda_1)|(\theta=0)=K_{\sigma,\lambda_1} \qquad K_2 f_{\theta\theta}(\theta,\lambda_2)|(\theta=0)=K_{\sigma,\lambda_2}$$

$$K_1 f_{r\theta}(\theta,\lambda_1)\big|(\theta=0)=K_{\tau,\lambda_1} \qquad K_2 f_{r\theta}(\theta,\lambda_2)\big|(\theta=0)=K_{\tau,\lambda_2}$$

(11)

These parameters ($K_{\sigma,\lambda1}$, $K_{\sigma,\lambda1}$, $K_{\tau,\lambda1}$, $K_{\tau,\lambda2}$) are controlled from K_1 and K_2, so the singular stress field is also controlled by the two real parameters. Integral path for RWCIM is shown in Fig 5. Plane strain condition was selected for carrying out the linear elastic analyses in MSC Marc software. Representation of the selected mesh pattern for developing these analyses is shown in Fig 6. Around the interface corner edge eight-node elements were utilized, while for other regions away from the interface corner edge, four-node elements were selected. Minimum mesh size (e_{min}) was: 1.882E-6 mm ($1/3^{12}$ mm).

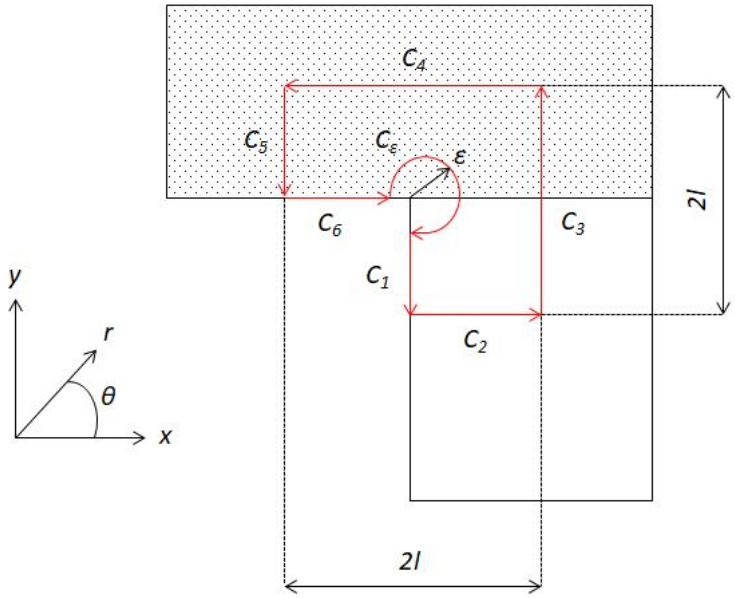

Figure 5. Integral path C for RWCIM ($C=C_1+C_2+C_3+C_4+C_5+C_6+C_\varepsilon$).

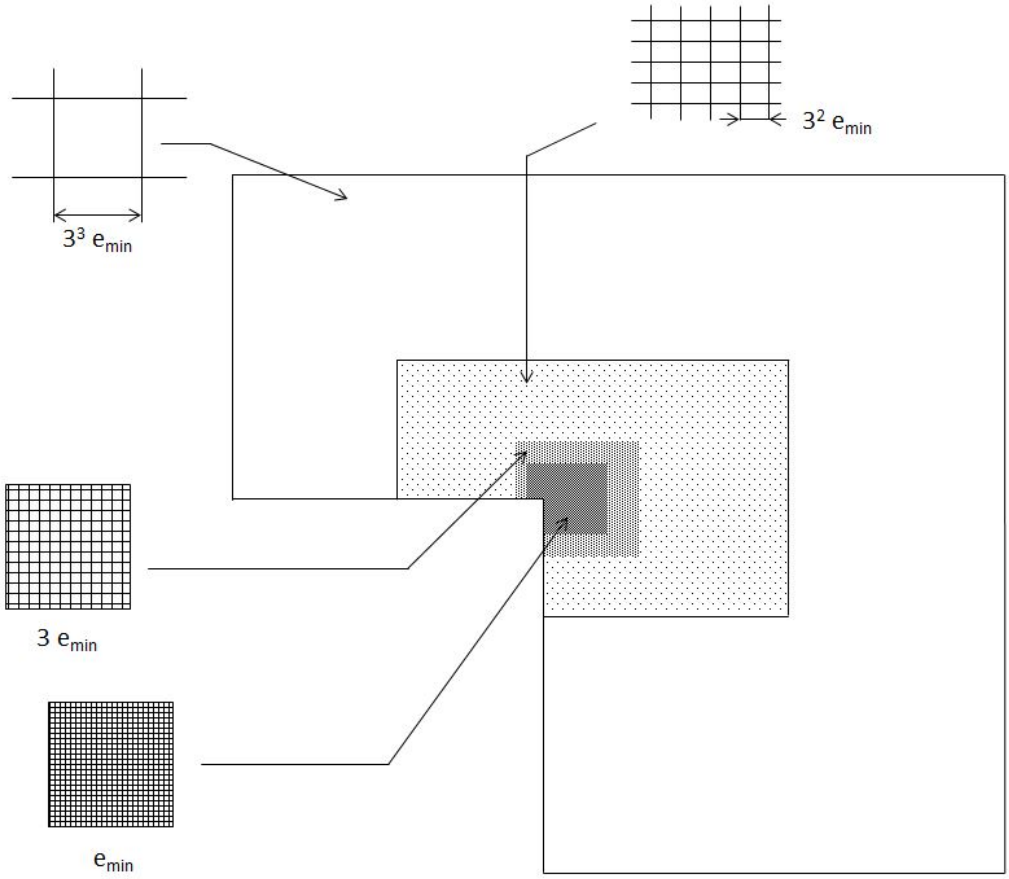

Figure 6. Mesh pattern near the interface edge corner.

4. Calculation of the reference solution

Singular stress distribution on the interface near the edge corner for Model 1 by mean of the RWCIM is shown in Fig 7. From σ_y equation ($\sigma_y = \frac{1.32}{r^{0.3494}} - \frac{0.08631}{r^{0.00000806}}$), $K^*_{\sigma,\lambda1}$ = 1.32 [MPa·mm$^{1-\lambda1}$] and $K^*_{\sigma,\lambda2}$ = -0.086 [MPa·mm$^{1-\lambda2}$] are obtained. While from τ_{xy} equation ($\tau_{xy} = -\frac{0.5211}{r^{0.3494}} - \frac{0.0001407}{r^{0.00000806}}$), $K^*_{\tau,\lambda1}$ = -0.521 [MPa·mm$^{1-\lambda1}$] and $K^*_{\tau,\lambda2}$ = -0.0001407 [MPa·mm$^{1-\lambda2}$] are obtained. In the same way, λ_1 = 0.651 and λ_2 = 0.999. Finite elements stress distributions are $\sigma^*_{y0,FEM}$ = 238.835 [MPa] and $\tau^*_{xy0,FEM}$ = -97.637 [MPa]. Material properties for SikaPower®-1548 and AISI 4140 are summarized in Table 2.

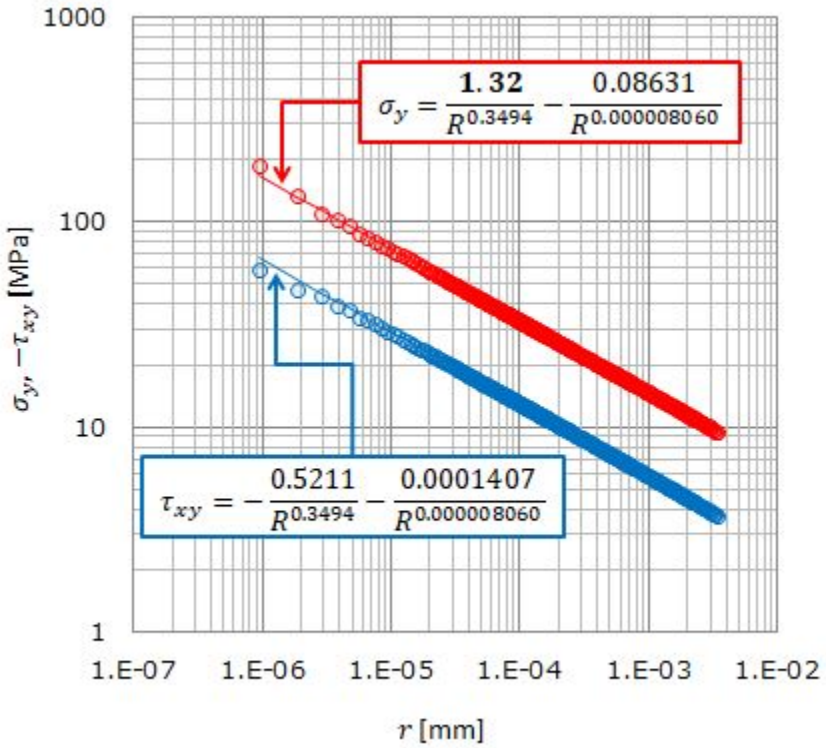

Figure 7. Singular stress distribution on the interface near the edge corner for Model 1.

Table 2. Material properties of SikaPower®-1548 and AISI 4140, material combination of Model 1 and Model 3.

Material	E (GPa)	υ	α	β	λ_1	λ_2
AISI 4140	210.0	0.3	-0.990	-0.170	0.651	0.999
SikaPower®1548	1.0	0.396				

Singular stress distribution on the interface near the edge corner for Model 2 using RWCIM is shown in Fig 8. From σ_y equation ($\sigma_y = \frac{2.030}{r^{0.3366}} - \frac{0.3029}{r^{0.00009136}}$), $K^*_{\sigma,\lambda1}$ = 2.030 [MPa·mm$^{1-\lambda1}$] and $K^*_{\sigma,\lambda2}$ = -0.303 [MPa·mm$^{1-\lambda2}$] are obtained. While from τ_{xy} equation ($\tau_{xy} = -\frac{0.7534}{r^{0.3366}} - \frac{0.001572}{r^{0.00009136}}$), $K^*_{\tau,\lambda1}$ = -0.753 [MPa·mm$^{1-\lambda1}$] and $K^*_{\tau,\lambda2}$ = -0.001572 [MPa·mm$^{1-\lambda2}$] are obtained. Being λ values: λ_1 = 0.663 and λ_2 = 0.999. While the finite elements stress distributions are: $\sigma^*_{y0,FEM}$ = 291.581 [MPa] and $\tau^*_{xy0,FEM}$ = -118.176 [MPa]. Materials properties of SikaPower®-1511 adhesive and AISI 4140 adherent are summarized in Table 3.

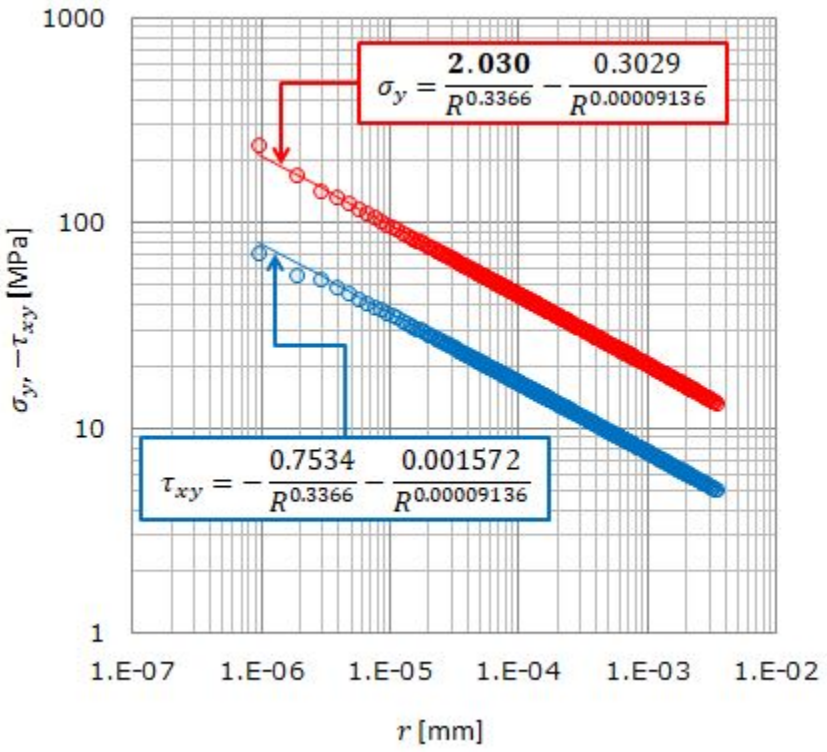

Figure 8. Singular stress distribution on the interface near the edge corner for Model 2.

Table 3. Material properties of SikaPower®-1511 and AISI 4140, material combination of Model 2 and Model 4.

Material	E (GPa)	υ	α	β	λ_1	λ_2
AISI 4140	210.0	0.3	-0.968	-0.202	0.663	0.999
SikaPower®1511	3.3	0.367				

5. Calculation of the unknown solution

After calculating the reference value of ISSF for Models 1 and 2, Eq 8 and Eq 9 can be used. As it is explained above, the results of Model 1 are the reference solutions to calculate the Model 3. And in the same way, the results of Model 2 are the reference solutions to calculate the Model 4. From Eq 8 and Eq 9 unknown values of the Model 3 and Model 4 are calculated. $K^*_{\sigma,\lambda1}$ and $K^*_{\tau,\lambda1}$ are the reference solutions of ISSF, while the unknown solutions have been designated as $K_{\sigma,\lambda1}$ and $K_{\tau,\lambda1}$. The stress distribution obtained by means of finite element method (FEM) is designated as $\sigma^*_{y0,FEM}$ and $\tau^*_{xy0,FEM}$ for the reference solution, and $\sigma_{y0,FEM}$ and $\tau_{xy0,FEM}$ for the unknown solution.

ISSF results for Model 3 are: $K_{\sigma,\lambda1}$ = 0.850 [MPa·mm$^{1-\lambda1}$] and $K_{\tau,\lambda1}$ = -0.335 [MPa·mm$^{1-\lambda1}$]. Stress distributions by FEM are: $\sigma_{y0,FEM}$ = 153.713 [MPa] and $\tau_{xy0,FEM}$ = -62.842 [MPa]. While ISSF results for Model 4 are: $K_{\sigma,\lambda1}$ = 2.626 [MPa·mm$^{1-\lambda1}$] and $K_{\tau,\lambda1}$ = -0.974 [MPa·mm$^{1-\lambda1}$]. Stress distributions by FEM are: $\sigma_{y0,FEM}$ = 377.115 [MPa] and $\tau_{xy0,FEM}$ = -152.835 [MPa].

Zhang et al [17,18] have demonstrated the effectiveness of the mesh-independent technique to calculate ISSF. In this way, adhesive strength can be shown as a constant value of critical ISSF ($K_{\sigma c}$=const.) [4,21,25]. Thus, the value of the ratios $\sigma_{y0,FEM}\Big/\sigma^*_{y0,FEM}$ and $\tau_{xy0,FEM}\Big/\tau^*_{xy0,FEM}$ are constant and independent of the mesh size. Table 4 shows FEM stress distributions and stress ratios obtained by different mesh sizes for Model 1 and Model 3. Table 5 shows FEM stress distributions and stress ratios obtained by different mesh sizes for Model 2

and Model 4. Ratios in both cases are constant, therefore the independence of the mesh is proven and the work is validated.

Table 4. FEM stress distributions obtained by different mesh sizes for Model 1 and Model 3.

$e_{min} = 1/3^{-12}$ mm			$e_{min} = 1/3^{-11}$ mm		
r	**$\sigma_{y,FEM}$ (MPa)**	**$\sigma_{y,FEM}/\ \sigma^*_{y,FEM}$**	**r**	**$\sigma_{y,FEM}$ (MPa)**	**$\sigma_{y,FEM}/\ \sigma^*_{y,FEM}$**
0	153.713	0.644	0	104.695	0.644
e_{min}	121.868	0.644	e_{min}	82.993	0.643
$2e_{min}$	85.741	0.643	$2e_{min}$	58.382	0.643
$3e_{min}$	70.185	0.643	$3e_{min}$	47.786	0.643
$4e_{min}$	66.776	0.643	$4e_{min}$	45.464	0.643
$5e_{min}$	61.477	0.643	$5e_{min}$	41.855	0.643

Table 5. FEM stress distributions obtained by different mesh sizes for Model 2 and Model 4.

$e_{min} = 1/3^{-12}$ mm			$e_{min} = 1/3^{-11}$ mm		
r	**$\sigma_{y,FEM}$ (MPa)**	**$\sigma_{y,FEM}/\ \sigma^*_{y,FEM}$**	**r**	**$\sigma_{y,FEM}$ (MPa)**	**$\sigma_{y,FEM}/\ \sigma^*_{y,FEM}$**
0	377.115	1.293	0	260.462	1.293
e_{min}	311.634	1.293	e_{min}	215.188	1.294
$2e_{min}$	224.026	1.294	$2e_{min}$	154.660	1.294
$3e_{min}$	185.257	1.294	$3e_{min}$	127.880	1.294
$4e_{min}$	175.21	1.294	$4e_{min}$	120.941	1.294
$5e_{min}$	162.349	1.294	$5e_{min}$	112.057	1.294

6. Comparison of the Models

As it is observed in Table 6, Model 3 (Figure 4) improves the behavior of the adhesive joint in terms of ISSF. All critical values ($K_{\sigma,\lambda1}$, $K_{\tau,\lambda1}$, $\sigma_{y0,FEM}$, $\tau_{xy0,FEM}$) have been reduced by 35.64% compared to Model 1. Only one adhesive has been used in Model 1, lower Young's modulus one. While in Model 3, two adhesives are used, lower Young's modulus adhesive in the corner and higher Young's modulus adhesive in the central area of the joint. The results show that the lower Young's modulus adhesive works better in the corner as long as the central area of the joint is more rigid.

Table 6. ISSF values of Model 1 (reference solution) and Model 3.

	Model 1		**Model 3**
$\mathbf{K^*_{\sigma,\lambda1}}$ **[MPa·mm$^{1-\lambda1}$]**	1.320	$\mathbf{K_{\sigma,\lambda1}}$ **[MPa·mm$^{1-\lambda1}$]**	0.850
$\mathbf{\sigma^*_{y0,FEM}}$ **[MPa]**	238.835	$\mathbf{\sigma_{y0,FEM}}$ **[MPa]**	153.713
$\mathbf{K^*_{\tau,\lambda1}}$ **[MPa·mm$^{1-\lambda1}$]**	-0.521	$\mathbf{K_{\tau,\lambda1}}$ **[MPa·mm$^{1-\lambda1}$]**	-0.335
$\mathbf{\tau^*_{xy0,FEM}}$ **[MPa]**	-97.637	$\mathbf{\tau_{xy0,FEM}}$ **[MPa]**	-62.842

Table 7 shows the results of Model 2 and Model 4. Opposite happens in comparison to Model 1 and Model 3. All critical values ($K_{\sigma,\lambda1}$, $K_{\tau,\lambda1}$, $\sigma_{y0,FEM}$, $\tau_{xy0,FEM}$) have been increased by 29.33% in Model 4 compared to Model 2. If only one adhesive is used, and this adhesive has enough Young's modulus, the result is better than if the same adhesive is used in the corners, and one adhesive with lower Young's modulus is used in the central area.

Table 7. ISSF values of Model 2 (reference solution) and Model 4.

	Model 2		Model 4
$K^*_{\sigma,\lambda1}$ [MPa·mm$^{1-\lambda1}$]	2.030	$K_{\sigma,\lambda1}$ [MPa·mm$^{1-\lambda1}$]	2.626
$\sigma^*_{y0,FEM}$ [MPa]	291.581	$\sigma_{y0,FEM}$ [MPa]	377.115
$K^*_{\tau,\lambda1}$ [MPa·mm$^{1-\lambda1}$]	-0.753	$K_{\tau,\lambda1}$ [MPa·mm$^{1-\lambda1}$]	-0.974
$\tau^*_{xy0,FEM}$ [MPa]	-118.176	$\tau_{xy0,FEM}$ [MPa]	-152.835

7. Conclusions

-The effect of Young's Modulus in terms of the ISSF is studied from the results obtained in the different models. Two models can be compared if the material combination in the edge corner is the same. In this way, Model 1 is compared with Model 3, while Model 2 is compared with Model 4.

-Model 3 shows a decrease of 35.64% of ISSF value compared with Model 1. Lower Young's modulus adhesive works better in the corner as long as the central area is covered by a higher Young's modulus adhesive.

-Model 4 shows an increase of 29.33% of the ISSF value compared with the reference Model 2. Combination of the higher Young's modulus adhesive in the corner and the lower Young's modulus adhesive in the central area is worse than applying a homogeneous layer of the higher Young's modulus adhesive only.

-Reciprocal work contour integral method (RWCIM) is a valid method to calculate the intensity of singular stress field (ISSF). However, it is a very complex method, and errors may occur during the calculation process. Reference values are calculated following RWCIM, being Model 1 and Model 2 the reference models.

-Calculating ISSF from the reference value and the stress ratio, it is just as accurate as using RWCIM (reciprocal work contour integral method). But it is necessary to know the reference value to be able to use it. In the same way, it is necessary to use the same mesh pattern, the same boundary conditions, and the same specimen configuration both in the reference and unknown solution. Model 3 and Model 4 are calculated by this method.

Acknowledgements

This research was supported by University Carlos III de Madrid under grants for the mobility of researchers, by Alvaro Alonso Barba Technological Institute of Chemistry and Materials (IAAB), and by Ministerio de Economia y Competitividad, Spain, under grants TRA2014-56471-C4-2-R.

Conflicts of Interest

The author(s) declared no potential conflicts of interest with respect to the research, authorship, and/or publication of this article.

Appendix A. Calculation of the reference solution by mean of Reciprocal Work Contour Integral Method (RWCIM)

ISSF value of the unknown solution ($K_{\sigma,\lambda1}$) can be easily calculated from the FEM stress ratio with Eq 8. However, in this case the reference solution is also unknown ($K^*_{\sigma,\lambda1}$), since there is no other work in the literature with the same material combination, specimen configuration and boundary conditions. Therefore, it is necessary to use RWCIM to calculate the reference value. This method is based on Betti's reciprocal theorem. By mean of Williams' eigenfunction expansion method, displacement and stress in the vicinity of the interface corner edge can be expressed as [25]:

$$\sigma_{ij} = \sum_{k=1}^{\infty} K_k f_{ij}(\theta, \lambda_k) r^{\lambda_k - 1} \tag{A.1}$$

$$u_i = \sum_{k=1}^{\infty} K_k g_i(\theta, \lambda_k) r^{\lambda_k} \tag{A.2}$$

Where K_k is obtained by RWCIM, f_{ij} and g_i are the eigenfunctions which depend on λ_k and θ angle. Eq A.3 is obtained from Betti's reciprocal theorem [25]:

$$\oint_C \left(\sigma_{ij} u_i^* - \sigma_{ij}^* u_i\right) \boldsymbol{n}_j ds = 0 \tag{A.3}$$

Where the normal vector of the boundary C is $\mathbf{n}_j$. σ^*_{ij} and u^*_i are the complementary stress and displacement. They satisfy the same equilibrium and constitutive relations as σ_{ij} and u_i, respectively. Both stress (σ^*_{ij}) and displacement (u^*_i) are expressed as it is shown in Eq A.4 and Eq A.5 respectively [25]:

$$\sigma_{ij}^{*} = \sum_{k=1}^{\infty} K_k^* f_{ij}(\theta, \lambda_k^*) r^{\lambda_k^* - 1} = \sum_{k=1}^{\infty} K_k^* f_{ij}(\theta, -\lambda_k) r^{-\lambda_k - 1} \tag{A.4}$$

$$u_i^{*} = \sum_{k=1}^{\infty} K_k^* g_i(\theta, \lambda_k^*) r^{\lambda_k^*} = \sum_{k=1}^{\infty} K_k^* g_i(\theta, -\lambda_k) r^{-\lambda_k} \tag{A.5}$$

Integral path C (C_1+C_2+C_3+C_4+C_5+C_6+C_ε) is shown in Figure 5. C_1 and C_6 lines are located along the stress free surface, and therefore, the integrals along these lines are zero. This assumes a change in Eq A.3, which can now be written as:

$$\int_{-\pi/2}^{\pi} \left(\sigma_{ij} u_i^* - \sigma_{ij}^* u_i\right) \varepsilon \boldsymbol{n}_j d\theta = \int_{C'} \left(\sigma_{ij} u_i^* - \sigma_{ij}^* u_i\right) \boldsymbol{n}_j ds \tag{A.6}$$

Not taking into account C_1 and C_6 makes that $C' = C_2 + C_3 + C_4 + C_5$. σ_{ij} and u_i located on the left side of the equation are shown in Eq A.1 and Eq A.2. While σ_{ij} and u_i located on the right side of the equation are the stress and displacement calculated by mean of FEM ($\sigma_{ij,FEM}$ and

$u_{i,FEM}$). σ^*_{ij} and u^*_i are given by Eq A.4 and Eq A.5. When $\varepsilon \to 0$, integral on the left side of the equation becomes constant. Following equation is used as K^*_k [25]:

$$1/K_k^* = \int_{-\pi/2}^{\pi} \left[f_{ij}(\theta, \lambda_k) g_i^*(\theta, \lambda_k^*) - f_{ij}^*(\theta, \lambda_k^*) g_i(\theta, \lambda_k) \right] \boldsymbol{n}_j d\theta \tag{A.7}$$

ISSF K_k is obtained from the following equation:

$$K_k = \int_{C'} \left(\sigma_{ij,FEM} u_{ik}^* - \sigma_{ijk}^* u_{i,FEM} \right) \boldsymbol{n}_j ds \tag{A.8}$$

Where $\sigma_{iik}^* = K_k^* f_{ii}(\theta, \lambda_k^*) r^{\lambda_k^* - 1}$ and $u_{ik}^* = K_k^* g_i(\theta, \lambda_k^*) r^{\lambda_k^*}$. RWCIM is a valid method to calculate the ISSF. However, it is also a very complex method and requires a large number of calculations (such as operations with matrix and numerical integration). Therefore, it is not a very practical method. The proposed method in section 5 to calculate the ISSF (from a reference solution of the ISSF) is just as accurate as the RWCIM, being more convenient and practical. In this method it is only necessary to focus on the results obtained by FEM at the corner point without risking of calculation errors.

5. References

[1] Banea MD, Da Silva LFM. Adhesively bonded joints in composite materials: an overview. Proc Inst Mech Eng Part L: J Mater: Des Appl 2009; 223: 1–18.

[2] Xará JTS, Campilho RDSG. Strength estimation of hybrid single-L bonded joints by the extended Finite Element Method. Compos Struct 2018; 183: 397-406.

[3] Li R, Noda NA, Takaki R, Sano Y, Takase Y, Miyazaki T. Most suitable evaluation method for adhesive strength to minimize bend effect in lap joints in terms of the intensity of singular stress field. Int J Adhes Adhes 2018; 86: 45-58.

[4] Noda NA, Li R, Miyazaki T, Takaki R, Sano Y. Convenient adhesive strength evaluation method in terms of the intensity of singular stress field. Int J Comput Methods 2018; 15(1): 1850085 01-30.

[5] Mintzas A, Nowell D. Validation of an Hcr-based fracture initiation criterion for adhesively bonded joints. Eng Fract Mech 2012; 80: 13-27.

[6] Wang CH, Rose LRF. Compact solutions for the corner singularity in bonded lap joints. Int J Adhes Adhes 2000; 20: 145-154.

[7] Goglio L, Rossetto M. Evaluation of the singular stresses in adhesive joints. J Adhes Sci Technol 2009; 23: 1441-1457.

[8] Galvez P, Abenojar J, Martinez MA. Durability of steel-CFRP structural adhesive joints with polyurethane adhesives. Compos Part B-Eng 2019; 165: 1-9.

[9] Martinez MA, Velasco F, Abenojar J, Pantoja M, Del Real JC. Analytical solution to calculate the stress distribution in pin-and-collar samples bonded with anaerobic adhesives (following ISO 10123 standard). Int J Adhes Adhes 2008; 28: 405-10.

[10] Li G, Lee-Sullivan P, Thring RW. Nonlinear finite element analysis of stress and strain distributions across the adhesive thickness in composite single-lap joints. Compos Struct 1999; 46: 395-403.

[11] Chiminelli A, Breto R, Izquierdo S, Bergamasco L, Duvivier E, Lizaranzu M. Analysis of mixed adhesive joints considering the compaction process. Int J Adhes Adhes 2017; 76: 3-10.

[12] Breto R, Chiminelli A, Lizaranzu M, Rodríguez R. Study of the singular term in mixed adhesive joints. Int J Adhes Adhes 2017; 76: 11-16.

[13] Fitton MD, Broughton JG. Variable modulus adhesives: an approach to optimized joint performance. Int J Adhes Adhes 2005; 25: 329-36.

[14] da Silva LFM, Lopes MJCQ. Joint strength optimization by the mixed-adhesive technique. Int J Adhes Adhes 2009; 29: 509-14.

[15] Carbas RJC, da Silva LFM, Critchlow GW. Adhesively bonded functionally graded joints by induction heating. Int J Adhes Adhes 2014; 48: 110-18.

[16] da Silva LFM, Rodrigues TNSS, Figueiredo MAV, de Moura MFSF, Chousal JAG. Effect of adhesive type and thickness on the lap shear strength. J Adhesion 2006; 82: 1091-115.

[17] Zhang Y, Noda NA, Takaishi K, Lan X. Effect of adhesive thickness on the intensity of singular stress at the adhesive dissimilar joint. J Solid Mech Mater Eng 2010; 4(10): 1467-79.

[18] Zhang Y, Noda NA, Wu PZ, Duan ML. A mesh-independent technique to evaluate stress singularities in adhesive joints. Int J Adhes Adhes 2015; 57: 105-17.

[19] Dundurs J. Discussion: ''edge-bonded dissimilar orthogonal elastic wedges under normal and shear loading''. Trans ASME J Appl Mech 1969; 36: 650-2.

[20] Noda NA, Miyazaki T, Li R, Uchikoba T, Sano Y. Debonding strength evaluation in terms of the intensity of singular stress at the interface corner with and without fictitious crack. Int J Adhes Adhes 2015; 61: 46-64.

[21] Bogy DB. Two edge-bonded elastic wedges of different materials and wedge angles under surface tractions. Trans ASME J Appl Mech 1971; 38: 377-86.

[22] Noda NA, Ren F, Takaki R, Wang Z, Oda K, Miyazaki T, Sano Y. Intensity of singular stress field over the entire bond line thickness range useful for evaluating the adhesive strength for plate and cylinder butt joints. Int J Adhes Adhes 2018; 85: 234-50.

[23] Noda NA, Takase Y. Generalized stress intensity factors of V-shaped notch in a round bar under torsion, tension, and bending. Eng Fract Mech 2003; 70: 1447-66.

[24] Carpenter WC. Insensitivity of the reciprocal work contour integral method to higher order eigenvectors. Int J Fracture 1995; 73: 93-108.

[25] Mintzas A, Nowell D. Validation of an Hcr – based fracture initiation criterion for adhesively bonded joints. Eng Fract Mech 2012; 80: 13-27.